PROCEEDINGS, 50th Workshop on Geothermal Reservoir Engineering
Stanford University, Stanford, California, February 10-12, 2025
SGP-TR-229

A Two-Stage Approach to Native State Modeling, and Insights from Production Modeling, of the Roosevelt Hot Springs Hydrothermal System

Aileen Zebrowski and Brian J. McPherson

Civil & Environmental Engineering, 110 Central Campus Drive, Suite 2000, University of Utah, Salt Lake City, UT 84112

b.j.mcpherson@utah.edu

Keywords: geothermal, hydrothermal, native state, production, thermo-hydrological modeling, Basin and Range, steam cap

ABSTRACT

Roosevelt Hot Springs (RHS), located near Milford, Utah, is a magmatic, structurally controlled hydrothermal system in the Basin and Range geological province. The Blundell geothermal power plant has been operating at this site for over 40 years, since 1984. Blundell produces more fluid from the reservoir than it reinjects, leading to a net decline in reservoir fluid and pressure. We hypothesize that this pressure drop is driving the growth of a subsurface steam cap. The purpose of this study is to quantitatively test that hypothesis via subsurface modeling, and to demonstrate how reservoir development has influenced formation and expansion of a subsurface steam cap.

The model developed in this study is a regional, three-dimensional, two-phase representation of the hydrothermal reservoir and its surrounding area. The modeling process consists of two main components: native state modeling and production modeling. The purpose of the native state modeling is to establish pre-production conditions in the simulated reservoir. To achieve this, it was necessary to further divide the native state modeling into two stages of development: an initialization stage and an activation stage. These two stages represent a step change in reservoir permeability, indicative of the transient nature of the system permeability over geological timescales. The native state model then serves as initial condition for the production model, which simulates 40 years of reservoir development and the effects of production and injection wells.

The primary conclusions of this modeling effort are 2-fold. The first key finding is that native state modeling requires a two-stage approach to replicate observed reservoir conditions. The intermediate permeability of the initialization stage enables high temperatures to be widely distributed at shallow depths. Meanwhile, the high reservoir permeability of the activation stage is essential to support geothermal production, and represents chemo-mechanical processes such as fault activation. Both stages are essential for developing the high-temperature, productive reservoir observed at RHS today, demonstrating the system's dynamic nature over geologic time. Thus, permeability changes must be considered when modeling hydrothermal systems over long timescales. Secondly, production modeling results reveal that the formation and expansion of a subsurface steam cap above the reservoir is in direct response to geothermal production activities, supporting our hypothesis.

1. INTRODUCTION

Roosevelt Hot Springs (RHS), a hydrothermal system near Milford in southwest Utah, is situated along the western foothills of the Mineral Mountains within the Basin and Range geological province, a region of tectonic extension faulting (Knudsen et el., 2019). The subsurface reservoir has peak temperatures between 250-270ºC, and is nestled at the intersection of two sub-vertical faults: the north-south trending Opal Mound Fault (OMF) and the east-west trending Mag Lee Fault (MLF) (Allis et al., 2015). Both faults terminate at this intersection, creating a series of fault splays to the north. The highly fractured reservoir is recharged by deep circulation of meteoric water from the Mineral Mountains, which is heated by a magmatic intrusion at depth, and then upwells along the OMF. The OMF acts as a hydraulic boundary and serves as a structural control for the system (Faulder, 1991). The fluid predominantly exits the system via a shallow outflow plume to the north at a rate of approximately 60 kg/s, and to a lesser extent via an outflow plume to the south (Allis et al., 2019; Zebrowski and McPherson, 2024). A map view and cross-section of the site is shown in Figure 1.

The RHS reservoir supplies heated fluid to the Blundell geothermal power plant, commissioned in 1984 (Allis et al., 2015; Zebrowski, 2024). The original power plant, which is still in use today, is a flash-steam plant that currently produces 23 MW of net electricity to the grid. In 2007, a binary cycle power plant was integrated into Blundell's operations, supplying an additional 10 net MWe. 85% of the produced geothermal fluid is reinjected, while the rest (approximately 3 billion lbs/yr) is lost due to evaporation at the cooling towers, resulting in a net pressure decline in the reservoir. Observed thermal ground and fumarolic activity is likely in response to this operation, and an increase in vertical extent of subsurface steam above the reservoir has also been observed (Allis and Larsen, 2012; Zebrowski, 2024; Zebrowski and McPherson, 2024). These observations have led to the hypothesis that pressure decline from geothermal production has caused the formation of a subsurface steam cap. To test this hypothesis, a subsurface model of RHS was constructed to observe the reservoir response to production activities. The model presented here is a portion of the thesis research conducted by Zebrowski (2024).

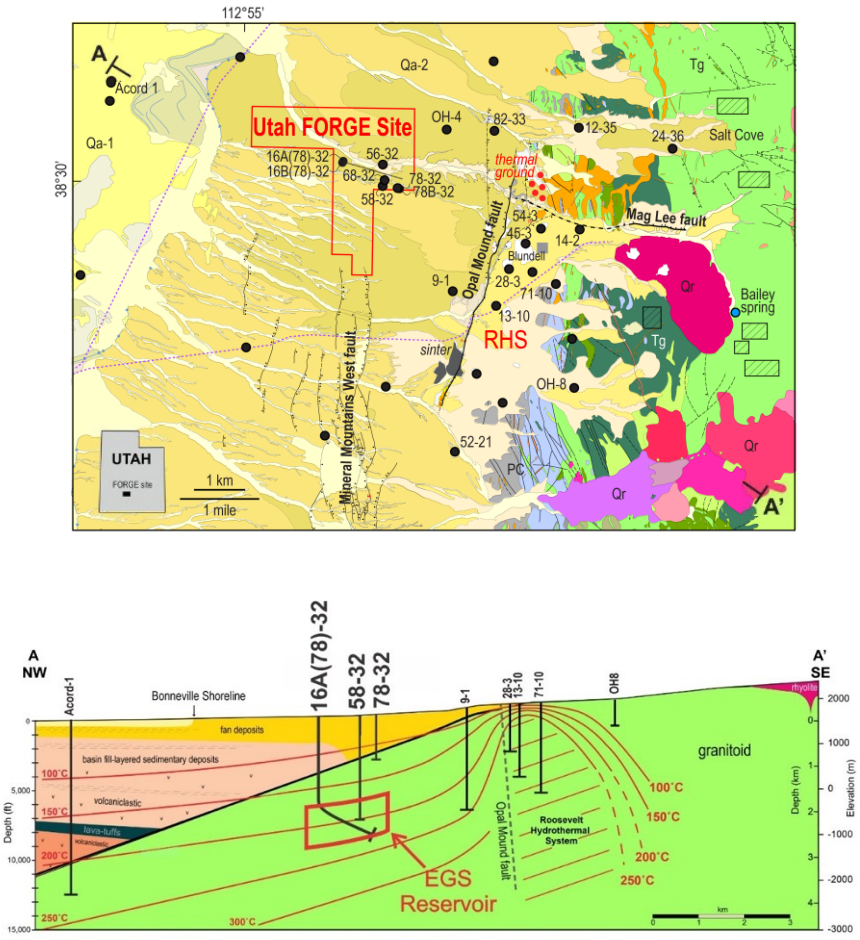

Figure 1: Site layout. A Map view (top) and cross-sectional view (bottom) of the Roosevelt Hot Springs and Utah FORGE site. Figure is updated from Moore et al. (2020).

1.1 RHS Reservoir Models

To inform the present study, four RHS models previously published in the literature were reviewed. Three of these models, constructed by Faulder (1991), Becker and Blackwell (1993), and Yu et al. (2021), are two-dimensional (2D), single-phase, regional, native state models. These studies follow a cross-section from the Mineral Mountains to the Milford Valley, with the reservoir located in-between. A fourth model, Yearley (1994), is a three-dimensional (3D), two-phase production model of RHS. However, the domain is restricted to the localized reservoir area.

The model presented in this study builds on these previous simulations by creating the first 3D, regional, two-phase model of the Roosevelt Hot Springs, incorporating both native state and production modeling (Zebrowski, 2024). By starting with a native state model, we ensure stability of the production model initial conditions, while the regional scale improves confidence in the selection of boundary conditions. This modeling approach also provides a mechanism to explore the subsurface steam cap under commercial production activities, while accounting for spatial heterogeneities in the third dimension, such as the distribution of faults and wells. Additionally, a novel approach to native state modeling was applied by splitting the model into two stages: an initialization stage and an activation stage. This two-stage approach represents a step-change permeability increase over geological time and is discussed further in Section 3.

2. MODEL SETUP

For this study, we developed a model of the Roosevelt Hot Springs system using TOUGH2 (Pruess et al., 2012). The model setup is described below, with a more detailed description presented in Zebrowski (2024).

2.1 Domain

The 3D model domain extends 20.5 km wide in the east-west direction, from the crest of the Mineral Mountains to the lowest point of the Milford Valley (at the Beaver River), 12.7 km in the north-south direction, reaching several km beyond the northern and southern ends of the OMF, and 6 km deep on average. The base of the model is fixed at -4 km above sea level (asl) while the top follows local surface topography (ranging from 1.5 to 2.46 km asl) (Topex, n.d.). The depth of the permeable upflow zone is estimated to be between 4 and 5 km, and the RHS magma source may lie as shallow as 5 to 8 km below the surface (Allis et al., 2019; Becker and Blackwell, 1993;

Faulder, 1991; Trow et al., 2019). Therefore, we suggest that a model depth of 4 to 6 km is reasonable. The orientation of the model follows the cardinal directions, which aligns closely with the major direction of topographic flow. The model extents are given in Table 1 and depicted in Figure 2 (Zebrowski, 2024).

Table 1: Domain extents used in the RHS model. Northing and easting values (UTM 12N) and elevation values (msl) are given for the minimum and maximum extents of the domain in each direction (Zebrowski, 2024).

	Minimum	Maximum
Northing (m)	4,255,049	4,267,778
Easting (m)	324,750	345,275.1
Elevation (msl)	-4,100	2,460

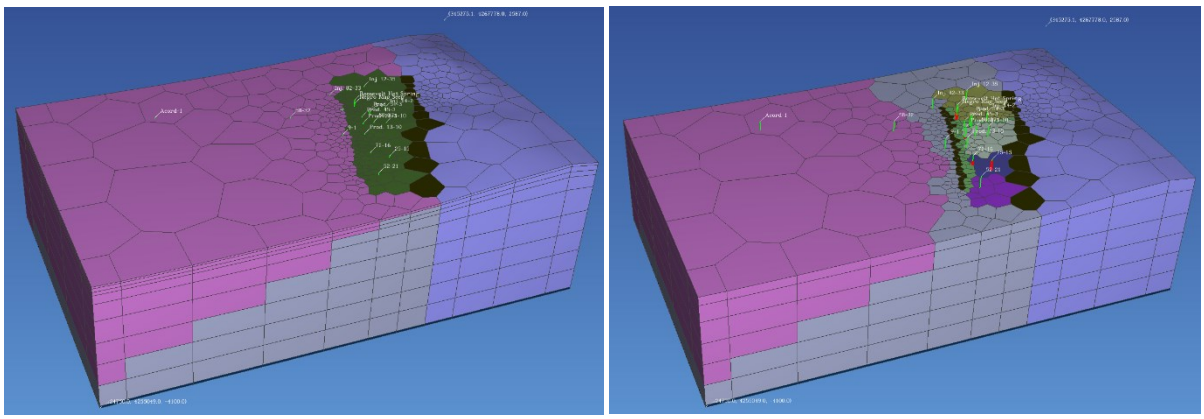

Figure 2: RHS model domain and material distribution. The left figure shows the entire domain, while the top three layers are removed in the right figure to display the reservoir material distribution. Each color represents a different material type. To see the full material distribution for the model layer by layer, see Zebrowski (2024).

2.2 Boundary Conditions

The model domain was carefully selected to reduce uncertainty around the boundary conditions. The lateral domain extents were all assumed to be no-flow boundaries by setting the eastern and western boundaries at regional topographic high and low points (hydraulic divides) and setting the northern and southern boundaries subparallel to the hydraulic gradient (Kirby et al., 2019; Zebrowski, 2024). The northern and southern boundaries extend several kilometers beyond the OMF to avoid localized lateral outflow from the reservoir.

The basal layer is also treated as a no-fluid-flow boundary due to decreasing permeability with depth, particularly approaching the magma chamber, which renders fluid flow negligible. The basal boundary does, however, need to account for geothermal heat inputs from depth, and the basal heat flux is not constant across the model domain. To account for this, we divided the basal layer into five regions, and named these regions (from west to east) as follows: Milford Valley, Acord-1, 58-32, Reservoir, and Mineral Mountains (MM). The heat flux values assigned to each region are 90, 100, 180, 500, and 210 mW/m², respectively, based on the regional Basin and Range heat flow and heat flux calculations made using the Acord-1, 58-32, and 24-36 well profiles, (Allis et al., 2019; East, 1981). The basal heat flux could not be directly calculated beneath the convecting geothermal reservoir, however, and consequently the reservoir heat flux was a variable used as part of the model calibration process. The delineation of these regions and their corresponding flux rates are shown in Figure 3 (Zebrowski, 2024).

The top boundary of the model is a fixed-state boundary defined by surface atmospheric conditions. For this model, values of 10°C and 101.3 kPa are applied across the entire ground surface. The complete model boundary conditions are summarized in Table 2 (Zebrowski, 2024).

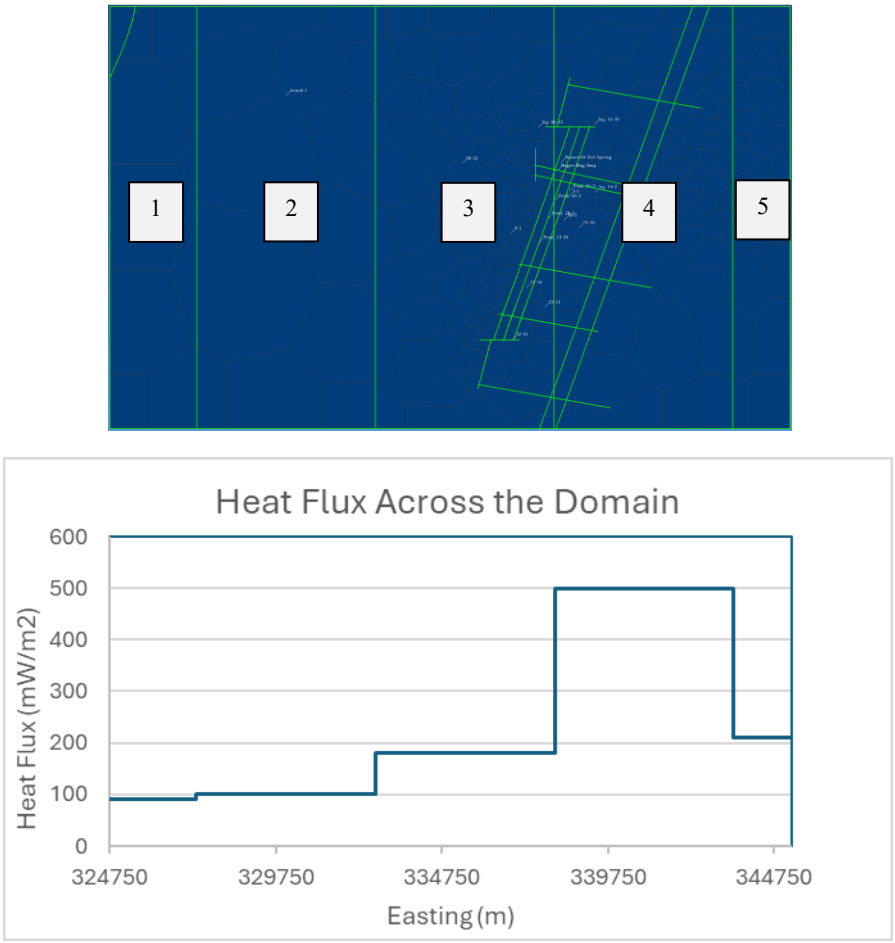

Figure 3: Basal heat flux regions. Top: Plan view of the basal layer, with the basal regions delineated by vertical green lines. From left to right the regions are numbered 1-5, and named, respectively: Milford Valley, Acord-1, 58-32, Reservoir, and MM. The additional green lines represent where the reservoir regions intersect with the basal layer. Bottom: The heat flux variation across the domain from east to west, corresponding to the regions 1-5 above (Zebrowski, 2024).

Table 2: Boundary and initial conditions used in the RHS model (Zebrowski, 2024).

Boundary	Boundary Condition	Initial Condition
Top	Fixed-State	P = 101.3 kPa T = 10°C
Bottom	No fluid flow Heat inputs (see Figure 3)	P = 101.3 kPa + (9.792 kPa/km)*depth T = 10°C + (45°C/km)*depth
All sides	No-flow	See Equations 1 and 2

2.3 Initial Conditions

A hydrostatic pressure gradient (9.792 kPa/km) and constant temperature gradient of 45°C/km were used to assign initial conditions to the native state model, based on the temperature profile in the Acord-1 well in the Milford Valley (Allis et al., 2019). The following linear functions were applied to the model domain to define the initial pressure (P_i) and temperature (T_i) distributions.

$$P_i = -18686 + 0.4185x - 9792z \quad (1)$$

$$T_i = -541.4 + 0.001923\text{x} - 0.045\text{z} \quad (2)$$

where x is the easting (m) and z is the elevation (msl). The initial conditions are summarized in Table 2 (Zebrowski, 2024).

Once the native state model reached conditions reasonably representative of the pre-production conditions in the reservoir, the pressure and temperature distributions of the native state model were used as the initial conditions for the reservoir model. This same method is used between the initialization and activation stages of the native state model, which are described in Section 3.

2.4 Domain Discretization

We discretized the model domain horizontally using a polygonal mesh, with additional refinement around the faults. This refinement increases the resolution in the reservoir, while maintaining a coarser grid away from the reservoir to ensure reasonable simulation run times. We discretized the domain vertically by layers, with increased refinement near the ground surface where the most significant activities take place (such as well production, steam cap formation, and lateral outflow). The bottom four layers of the domain are each 1 km thick. The five remaining layers vary in thickness based on the topography, but starting from 0 asl up to the ground surface, the layers have median thicknesses of approximately 1000 m, 500 m, 200 m, 200 m, and 100 m. An additional basal layer, 100 m thick, is added at the bottom of the domain and used to implement the basal boundary conditions (Zebrowski, 2024).

2.5 Geological Units

We also divided the model into regions based on the geological units. At the coarsest level, the domain predominantly consists of granitoid, topped with alluvial basin fill in the valley. The granitoid rock, however, can be subdivided into 3 main bodies based on permeability: the Mineral Mountain batholith to the east, the basement rock to the west, and the highly fractured reservoir in the center (along the Opal Mound and Mag Lee faults). Moreover, the permeability is not evenly distributed within the reservoir itself. According to Yearsley (1994), the greatest permeability is near the fault intersection. Based on this, and other well data, the reservoir was subdivided even further into five main regions: the permeable fault zones (along the OMF and MLF), the main reservoir (adjacent to the fault intersection), the lower (southern) reservoir, and the northern and southern peripheral regions (Allis et al., 2019; Faulder, 1994; Forrest, 1994). The OMF behaves like a combined conduit-barrier type fault (Caine et al., 1996), and thus the reservoir and permeable fault zone is bounded to the west by an impermeable fault material. A low permeability eastern reservoir boundary is also included, modeled after Becker and Blackwell (1993) and hypothesized to be formed by mineralization. Additionally, the reservoir is capped with cemented alluvium and self-sealed granitoid (Zebrowski, 2024). The distribution of different geological units can be seen in Figure 2.

2.6 Internal Boundaries

Shapefiles from the Utah FORGE repository (Podgorney, 2020) were used to demarcate the OMF, MLF, and the contact between the granitoid basement rock and the basin fill in the valley, with minor adjustments made to fit the model domain. A 300 m buffer zone on either side of the faults was used to delineate between the impermeable and permeable fault, with the size being selected based on the resolution of the mesh. The reservoir width was set to be a constant 2.5 km wide, based on estimates of 1-3 km in the literature and results from model calibration (Allis et al., 2019; Faulder, 1991; Wilson and Chapman, 1980; Zebrowski, 2024).

3. TWO-STAGE NATIVE STATE MODEL CALIBRATION

The purpose of creating a native state model was to establish stable initial conditions for the production model. To calibrate the native state model, various setup parameters were adjusted until the model results reasonably matched pre-production conditions. Calibrating the model, however, revealed that reservoir permeability is in fact transient over geological timescales.

While high permeability in the reservoir is expected based on production rates, flow tests, and previous models (Becker and Blackwell, 1993; Faulder, 1991, 1994; Yearsley, 1994; Yu et al, 2021), during calibration of the model it became apparent that initializing the native state model with permeabilities high enough to support geothermal production caused convection currents to form within the reservoir, which prevented high temperatures from being widely distributed at shallow depths. To address this issue, lower than expected permeabilities were tested in the reservoir. In doing so, it was found that an intermediate permeability (5×10^{-17} m² horizontally and 5×10^{-16} m² vertically) is required to form the observed pre-production temperature distribution in the reservoir. This is because the lower permeability increases the residence time and lowers the Rayleigh number (Ra), limiting convection currents (see Section 3.1) (Ingebritsen et al., 2006). When the reservoir permeability is too low (<~1×10^{-17} m²), however, heat transport is dominated by conduction rather than convection, an observation also noted by McKenna and Blackwell (2004) in their Dixie Valley model (Zebrowski, 2024).

While the native state model needs to be initialized with an intermediate permeability, it cannot simultaneously support geothermal production. This suggests that reservoir permeability has changed over time, evolving over the ~100,000 years represented in the native state model. To reflect this transient behavior, we introduced a step-change in permeability by dividing the model into two stages:

1. Initialization stage – A lower permeability stage that establishes near-pre-production temperature conditions in the reservoir.

2. Activation stage – A subsequent increase in permeability, likely due to fault activation, allowing the reservoir to support geothermal production.

The transient nature of the native state permeability is supported by several sources, which suggest possible oscillation between periods of high and low permeability in structurally controlled geothermal systems (Becker and Blackwell, 1993; Lynne et al., 2005; McKenna and Blackwell, 2004; Moore and Nielson, 1994; Nielson et al., 1986; Wannamaker et al., 2021). These sources suggest that permeability is initially introduced due to movement along the faults, but the permeability self-seals over time through mineral deposition. Faults and fractures may later be reactivated by further geological activity, reinstating permeability. This process is known as fault valving, and episodic seismic swarms observed in the Mineral Mountains indicate that such behavior is likely present here (Mesimeri et al., 2021; Sibson, 2014; Wannamaker et al., 2021). As such, this two-stage native state model represents a single period of permeability oscillation. This approach allows the model to replicate high, widely distributed shallow temperatures, while establishing sufficient permeability to support geothermal production (Zebrowski, 2024).

3.1 Convection

To understand why convection currents occur when the native state is initialized with a high reservoir permeability, the Rayleigh number (Ra) is considered. Convection occurs when Ra is above a critical threshold, and can be calculated via the Bousinesq approximation (Ingebritsen et al., 2006) as:

$$Ra = \frac{\alpha_w \rho_w^2 c_w g k L (T_L - T_U)}{\mu_w K_m} \quad (3)$$

where α_w is thermal expansivity, ρ_w is density, c_w is specific heat, g is gravitational acceleration, k is permeability, L is the characteristic length, $(T_L - T_U)$ is the temperature difference, μ_w is dynamic viscosity, and K_m is thermal conductivity. These parameters influence convection (Zebrowski, 2024).

By looking at the influencing parameters, it is evident that higher permeabilities lead to a higher Ra. This is why convection currents occur less at lower permeabilities, and why a lower permeability initialization stage is necessary. When the permeability increases during activation, it might be expected that convection currents will start to form at that point. However, the temperature difference across the reservoir is also proportional to Ra, and after initialization the temperature gradient in the hydrothermal reservoir decreases. It is for this reason that the two-stage approach to the native state model is ideal for alleviating convection and allowing the system to achieve a wide distribution of very high temperatures at shallow depths (Zebrowski, 2024).

3.2 Simulation Duration

No predetermined simulation length was used for the native state modeling, rather the system was allowed to evolve until a good temperature match with the pre-production well profiles was achieved. To do this across two stages, the selection of the initialization period end time must consider how the fluid and heat distribution will evolve after introducing permeability into the reservoir. In this case, the optimal initialization stage duration was selected to be 95,000 years, at which point widely distributed high temperatures were observed at shallow depths, despite the peak heat still being too far east. When permeability was introduced following activation, however, it accelerated the westward spreading of hot fluid, and after 10,500 more simulated years, the reservoir temperature distribution closely matched the pre-production well profiles. The evolution of the native state model is shown in Figure 4 (Zebrowski, 2024).

The 10,500-year duration of the activation stage aligns with constraints presented in the literature. Typical Basin and Range faults experience large earthquakes every 1,000-20,000 years, which help prevent self-sealing (McKenna and Blackwell, 2004). At RHS specifically, the latest observed displacement across the OMF occurred during the late Pleistocene (Knudsen et al., 2019), while episodic hot spring discharge at the Opal Mound last occurred 1,600 years ago (Lynne et al., 2005). The timing of activation in the native state model fits within these constraints, suggesting that chemo-mechanical factors, such as earthquakes, contributed to reservoir activation (Zebrowski, 2024).

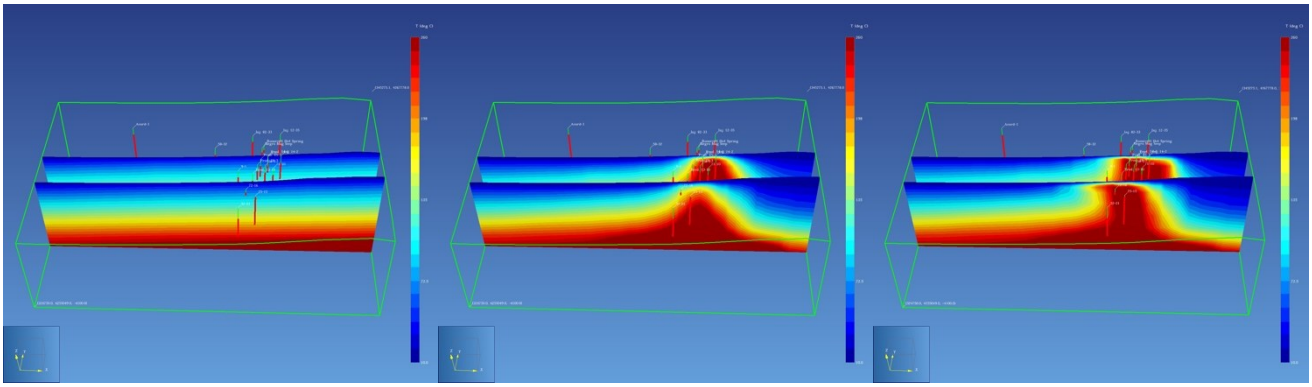

Figure 4: The native state model temperature distribution at, from left to right, initialization (t=0 yrs), activation (t=95,000 yrs), and when production begins (t=105,500 yrs) (Zebrowski, 2024). This view shows two vertical slice planes through the domain, from west to east. The color scale represents temperature and goes from 10°C (blue) to 260+°C (red).

3.3 Material Properties

The calibrated material properties for both the initialization and activation stages are summarized in Tables 3-4. The only difference between the initialization and activation stages is the permeability (and corresponding porosity) of the reservoir materials. Justification for these choices are described in Zebrowski (2024) based on data from numerous sources (Allis et al., 2019; Bamford et al., 1980; Becker and Blackwell, 1993; Faulder, 1991, 1994; Finnila et al., 2021; Gwynn et al., 2019; Podgorney et al., 2021; Mason, 1998; Moore et al., 2018, 2019; Nielson et al., 1986; Yearsley, 1994; Yu et al., 2021).

Table 3: Native state initialization stage material properties. These are the material properties for each material type / region in the RHS model. The eastern reservoir boundary is assigned to the impermeable fault material, and any self-sealed material is assigned as basement granitoid (Zebrowski, 2024).

Material Type	Horizontal Permeability (m^2)	Vertical Permeability (m^2)	Porosity	Thermal Conductivity (W/m·K)	Specific Heat (J/kg·K)	Density (kg/m^3)
Alluvium	1.00E-14	1.00E-16	0.2	1.6	1,000	2,400
Granitoid - Basement	4.70E-17	4.70E-17	0.01	2.5	1,000	2,750
Granitoid - MM	5.00E-16	5.00E-16	0.01	2.5	1,000	2,750
Fault - Impermeable	1.00E-18	1.00E-18	0.005	2.5	1,000	2,750
Fault - Permeable	1.00E-16	1.00E-15	0.02	2.5	1,000	2,700
Reservoir - Main	5.00E-17	5.00E-16	0.01	2.5	1,000	2,700
Reservoir - Lower						
Periphery - South						
Periphery - North						
Caprock	1.00E-14	1.00E-17	0.05	1.6	1,000	2,400
Basal	0	0	0	2.5	1,000	2,750

Table 4: Native state activation stage material properties. These are the material properties for each material type / region in the RHS model. The eastern reservoir boundary is assigned to the impermeable fault material, and any self-sealed material is assigned as basement granitoid (Zebrowski, 2024).

Material Type	Horizontal Permeability (m^2)	Vertical Permeability (m^2)	Porosity	Thermal Conductivity (W/m·K)	Specific Heat (J/kg·K)	Density (kg/m^3)
Alluvium	1.00E-14	1.00E-16	0.2	1.6	1000	2400
Granitoid - Basement	4.70E-17	4.70E-17	0.01	2.5	1000	2750
Granitoid - MM	5.00E-16	5.00E-16	0.01	2.5	1000	2750
Fault - Impermeable	1.00E-18	1.00E-18	0.005	2.5	1000	2750
Fault - Permeable	5.00E-15	5.00E-14	0.02	2.5	1000	2700
Reservoir - Main	2.50E-15	2.50E-14	0.015	2.5	1000	2700
Reservoir - Lower	1.00E-15	1.00E-14	0.015	2.5	1000	2700
Periphery - South	5.00E-16	5.00E-15	0.01	2.5	1000	2700
Periphery - North	5.00E-16	5.00E-15	0.012	2.5	1000	2700
Caprock	1.00E-15	1.00E-17	0.05	1.6	1000	2400
Basal	0	0	0	2.5	1000	2750

4. NATIVE STATE MODEL RESULTS AND DISCUSSION

4.1 Pre-Production Well Profiles

The native state model was calibrated to match the pre-production temperature profile within the reservoir, as shown in Figure 5. Most reservoir wells show a reasonable match, except for injection well 12-35 in the northern periphery, where the temperature is significantly higher in the model than was measured.

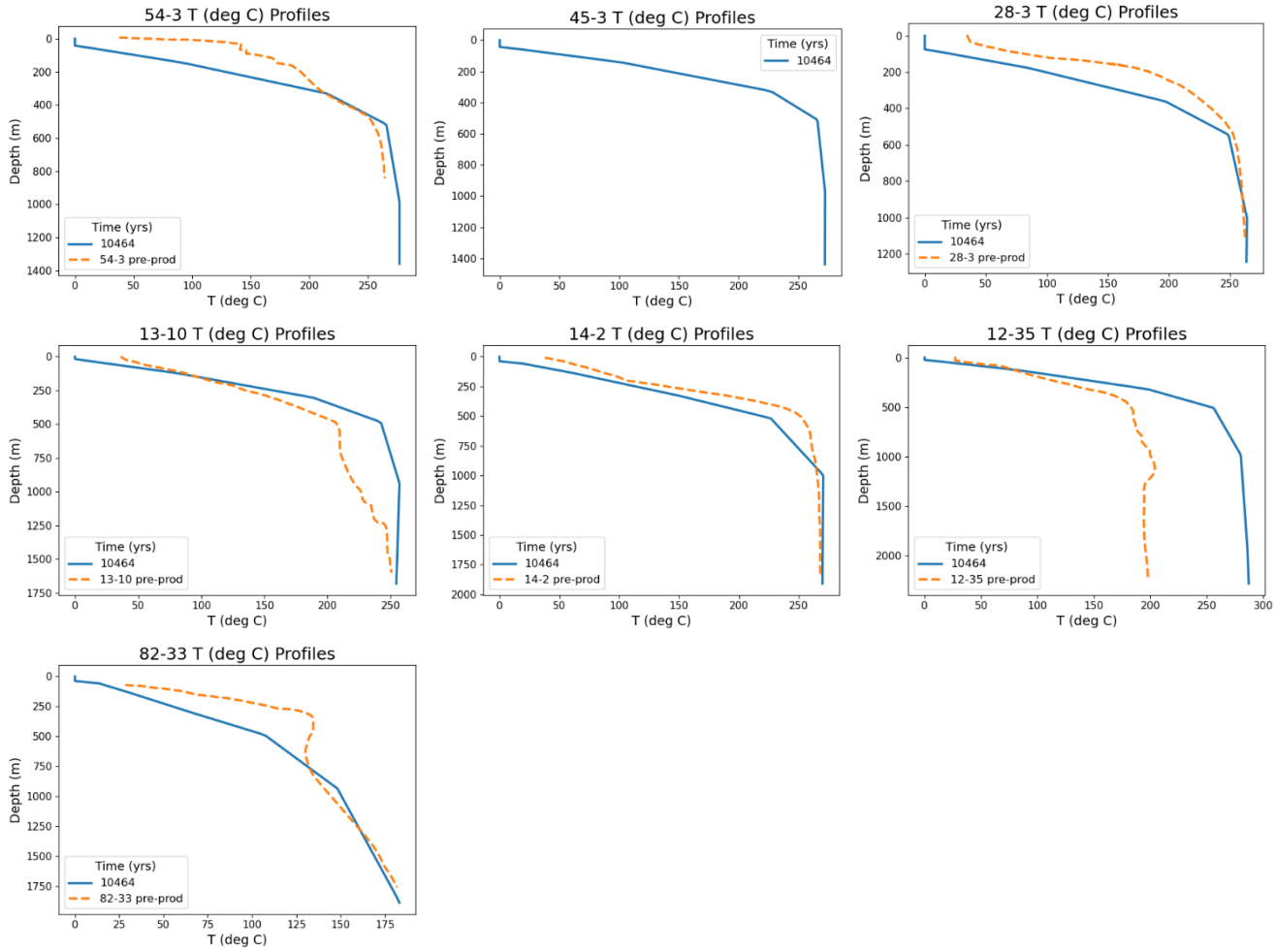

Figure 5: Native state well temperature profiles after 10,464 years of activation (solid blue lines) compared to the pre-production well temperature profiles (dashed orange lines). The production wells are first, followed by the injection wells. Well 45-3 has no pre-production data because it was drilled after production began (to replace well 35-3) (Zebrowski, 2024).

4.2.1 Reservoir Permeability

The impact bulk reservoir permeability has on the native state simulation results was discussed previously in Section 3 via the two-stage model design. In addition to bulk permeability, however, anisotropy in the reservoir also plays a role. The relative distribution of vertical to horizontal permeability within the reservoir significantly impacts upflow, and the height and evenness of the temperature distribution. It was observed that the upwelling of high temperatures to shallow depths improved when the vertical permeability was 1 to 2 orders of magnitude greater than the horizontal permeability. A 10:1 vertical to horizontal permeability ratio was ultimately selected during calibration and was maintained across all reservoir materials (Zebrowski, 2024).

The incorporation of a low permeability eastern reservoir boundary was also critical to achieving high temperature reservoir conditions. The use of such a boundary is based on the model used by Becker and Blackwell (1993) and is crucial for promoting deep circulation of the Mineral Mountain recharge and the subsequent upflow of heated fluids within the reservoir. Without this low-permeability boundary, unheated water can laterally infiltrate the main reservoir before absorbing deep heat. While this eastern boundary is not based on a structural feature like the OMF to the west, Becker and Blackwell (1993) justified this boundary by citing mineral deposition at the periphery of the reservoir (Lippmann and Bodvarsson, 1985; Zebrowski, 2024).

The presence of a caprock is also necessary for keeping the fluid and heat within the reservoir during the activation stage. At RHS, there is not a true caprock but rather cemented alluvium and self-sealed granitoid that effectively seals the top of the reservoir (Bamford et al., 1980; Glenn and Hulen, 1979; Wilson and Chapman, 1980). A low vertical caprock permeability improves heat retention in the reservoir, while a higher horizontal permeability allows the outflow of thermal fluid through the alluvium. To create this effect, the cemented alluvium caprock was assigned a vertical to horizontal permeability ratio matching that of the valley alluvium (1:10), but at 1 order of magnitude smaller (Zebrowski, 2024).

4.2.2 Mineral Mountain Permeability

Reservoir temperatures are highly sensitive to the permeability in the Mineral Mountains, which was also concluded by Faulder (1991). Previous models have constrained the MM permeability to be between zero and two orders of magnitude greater than that of the granitoid basement rock to the west. When the MM permeability is too high, the residence time is too short to heat the shallow reservoir. Conversely, if the MM permeability is too low, the fluid heats up at depth but insufficient volumes of fluid are transported up into the reservoir (Zebrowski, 2024).

The optimal permeability range for the Mineral Mountains was found to be extremely limited, and is set here at 5 x 10^{-16} m², with poor model behavior observed at other permeabilities. This falls within the range used by Becker and Blackwell (1993) (1 x 10^{-16} – 1 x 10^{-15} m²) and Faulder (1991) (5 x 10^{-17} m² & 5 x 10^{-16} m²). It also falls perfectly within the narrow bulk permeability range identified by McKenna and Blackwell (2004) as being suitable for geothermal systems in the Basin and Range (1 x 10^{-16} m²- 5 x 10^{-16} m²) (Zebrowski, 2024).

4.2.3 Reservoir Basal Heat Flux

Basal heat flux is a critical model variable that can drastically affect the temperature distribution across the region. The basal heat flux is reasonably well constrained across most of the domain based on calculations by Allis et al. (2019). However, the basal heat flux beneath the reservoir cannot be estimated in the same way because the reservoir exhibits a convective temperature profile. The initial estimate of the reservoir basal heat flux was 240 mW/m², slightly greater than the literature values for nearby wells. However, during calibration, this heat flux value had to be increased to 500 mW/m² to achieve the necessary high temperatures in the shallow reservoir. Iterations where the reservoir basal heat flux was set below this could not achieve the expected shallow heat distribution (Zebrowski, 2024).

Increasing the reservoir basal heat flux improved calibration of the model relative to the Faulder (1991) and Becker and Blackwell (1993) models, which never assigned a basal heat flow value greater than 150 mW/m², leading to low reservoir temperatures. One possible reason for the high reservoir basal heat flux is due to localized effects of the magma heat source at depth, as suggested by magnetotellurics (Wannamaker et al., 2021). Analogous conditions are seen at the Lassen geothermal system (Ingebritsen et al., 2006; Sorey and Colvard, 1994) where highly concentrated heat flux is also observed. Alternatively, the circulating fluid may follow a deeper or wider path than proposed in the current model, resulting in greater heat mining. These hypotheses are discussed in greater detail in Zebrowski (2024).

5. PRODUCTION MODELING

Once the native state model was calibrated, we ran a 40-year production model using the native state results as initial conditions. To run the production model, injection and production rates were turned on in the wells. There are four production wells located in the main reservoir (13-10, 28-3, 45-3, 54-3), one injection well also located in the main reservoir (14-2), and two injection wells located in the northern periphery (12-35 and 82-33). Approximate injection and production rates at these seven wells were provided by Allis and Larsen (2012) and are used here. Two new wells have been put into operation since that study (one injection and one production), but without knowledge of the flow rates at these newer wells, they have been neglected in this model. The well locations are shown in Figure 1, and the injection/production rates are summarized in Table 5 (Zebrowski, 2024). The rest of the production model setup is the same as the activation stage model.

Table 5: Well injection rates and fluid enthalpy used in the RHS model. Injection rates for each well are estimated based on data supplied in Allis and Larsen (2012). Negative injection rates indicate production (Zebrowski, 2024).

Well ID	Injection Rate (kg/s)	Injectate Enthalpy (J/kg)
13-10	-72.14	N/A
28-3	-72.14	
45-3	-72.14	
54-3	-72.14	
14-2	170.9	746,000 <7.253e8 seconds 443,000 >7.253e8 seconds
12-35	36.6	
82-33	36.6	

5.1 Steam Cap Formation

During production, a steam cap formed over the reservoir, as expected per our hypothesis. The steam initially appeared over the OMF before expanding over the MLF, main reservoir, and northern periphery, gradually extending deeper as well. The steam cap distribution after 40 years is shown in Figure 6 (Zebrowski, 2024).

Although there is considerable uncertainty about the exact degree and extent of steam formation, the model results show promising signs. First, the area where steam initially forms aligns with a documented two-phase fluid zone over well 54-3 (Simmons et al., 2021). Additionally, the modeled steam cap extends beneath the steaming ground in the northern periphery, supporting the influence of subsurface steam on evolving surface features (Zebrowski and McPherson, 2024). The way these subsurface characteristics manifest at the surface depends on smaller-scale permeability variations, such as fault splays, which are not explicitly included in this model (Zebrowski, 2024).

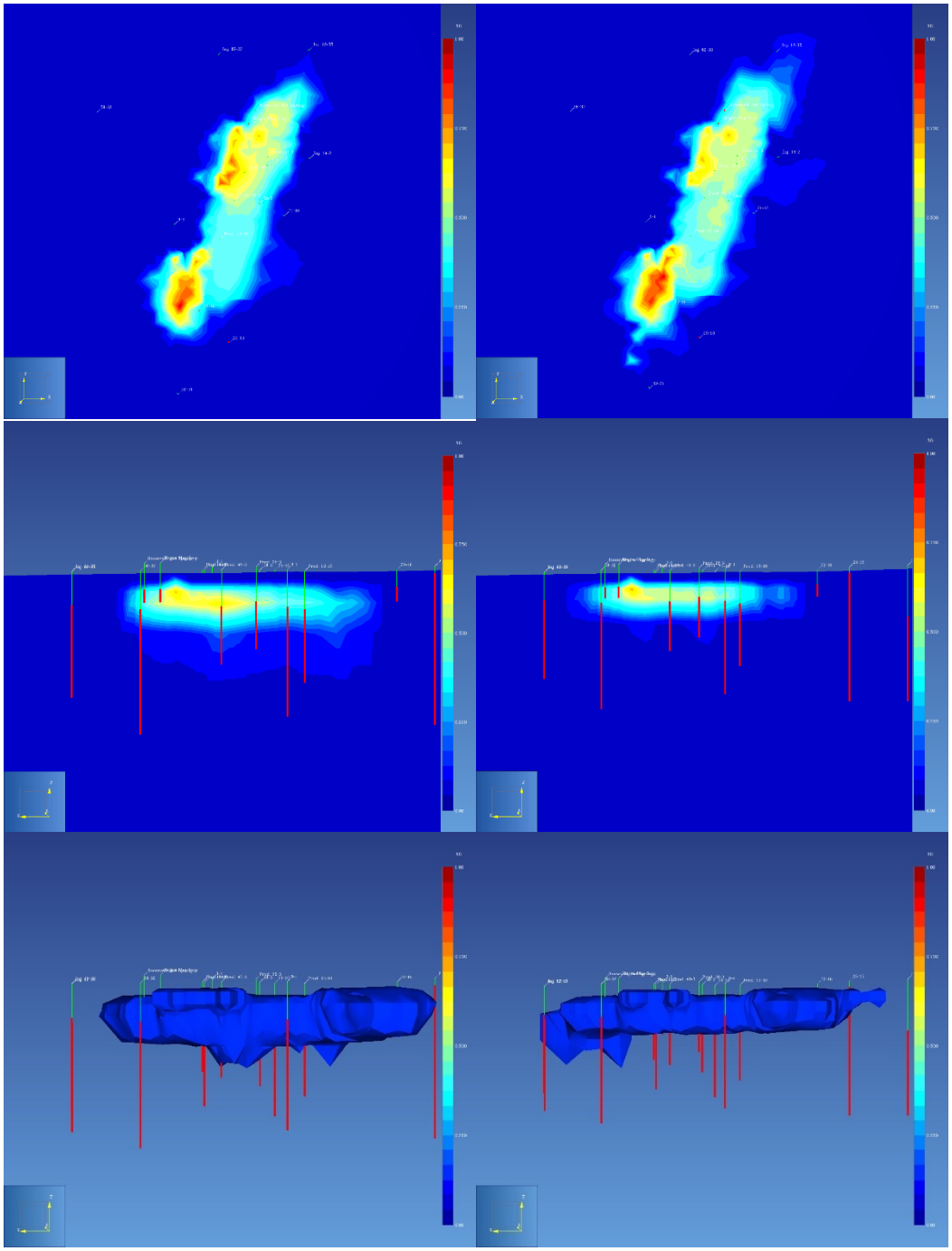

Figure 6: Steam cap distribution at Roosevelt Hot Springs after 40 years. Right: base case permeability. Left: higher reservoir permeability case. Top: plan view slice at 1,500 msl (shown from west to east). Middle: vertical slice at 338,400 m easting (shown from north to south). Bottom: steam isosurface (north to south). The color scale represents gas saturation and goes from 0 (blue) to 1 (red) (Zebrowski, 2024).

5.2 Production Model Well Profiles

To monitor the effects of production on the geothermal reservoir, the evolution of the well temperature profiles are plotted in Figure 7. A decrease in all the well temperatures is observed over time, with injection well 14-2 experiencing the most significant decline (since it accepts the largest volume of injectate). Over 40 simulated years, temperatures dropped by 10°C or less in each well, except 14-2 which dropped by 60°C. The modeled temperature declines in the production wells are similar to, or less than, those reported by Allis and Larsen (2012) and Simmons et al. (2021), indicating that this model has reasonable, though slightly optimistic, thermal recharge rates. The post-production temperatures at the injection wells, meanwhile, are unknown, so the model results cannot be compared (Zebrowski, 2024).

To discern the relationship between reservoir pressure and steam cap formation, the pressure in the wells was monitored over time (Figure 8). All the production well results show a decline in pressure, with the greatest pressure drop occurring during early time. The total pressure decline in the wells is approximately 3.5 - 4 MPa after 40 simulated years, which is only slightly less than the 4 MPa estimated by Allis and Larsen (2012) (after 27 years of production). The injection wells, meanwhile, have elevated pressures, and exhibit an immediate pressure spike followed by a decline from this peak (Zebrowski, 2024). The steam cap extents (Figure 6) correspond to this observed pressure distribution, with steam forming over the reservoir around the production wells but not at the injection wells where there's been a net increase in pressure.

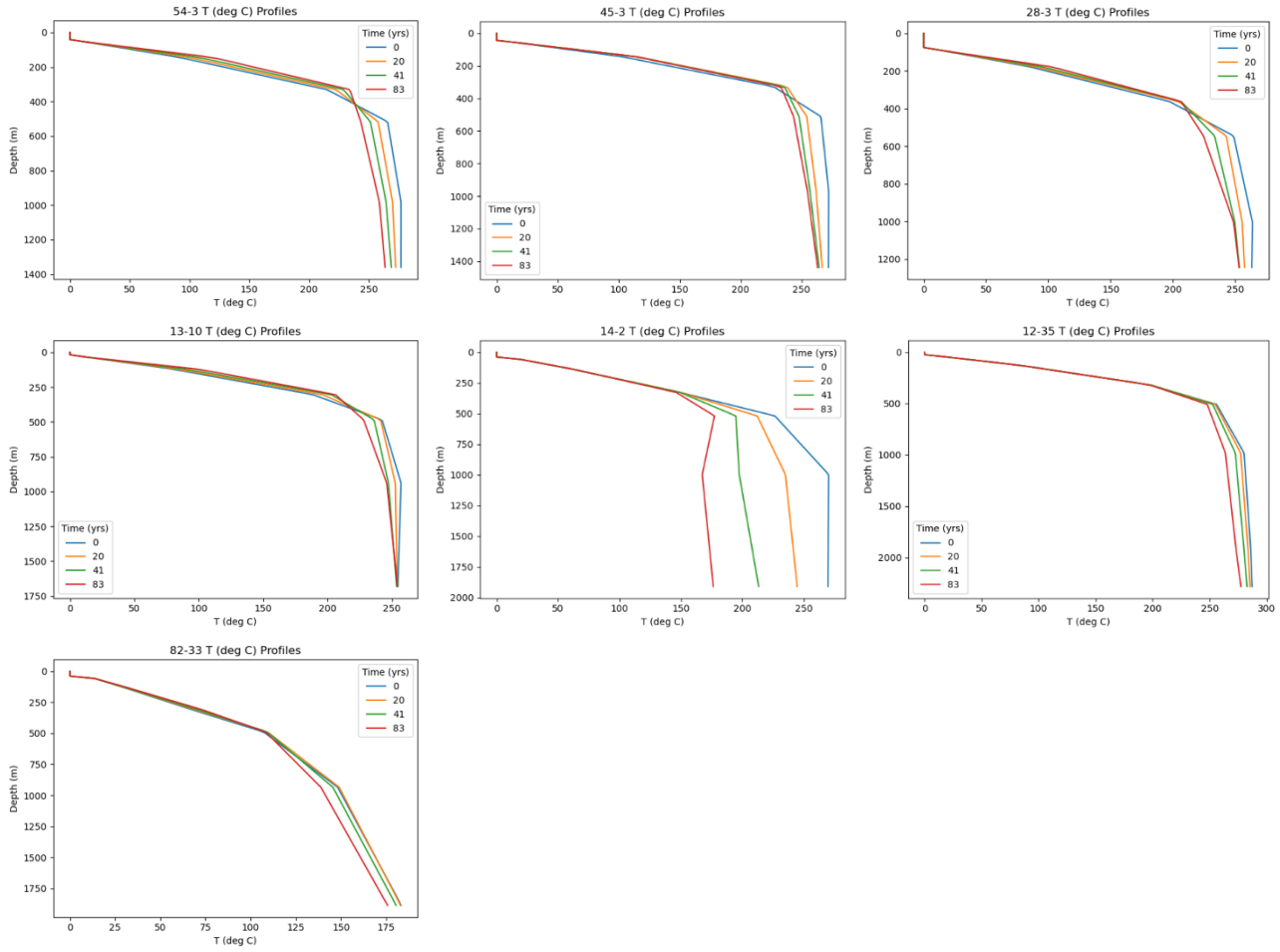

Figure 7: Production model temperature profiles in each well after 0, 20, 41, and 83 simulated years. The production wells are first, followed by the injection wells (Zebrowski, 2024).

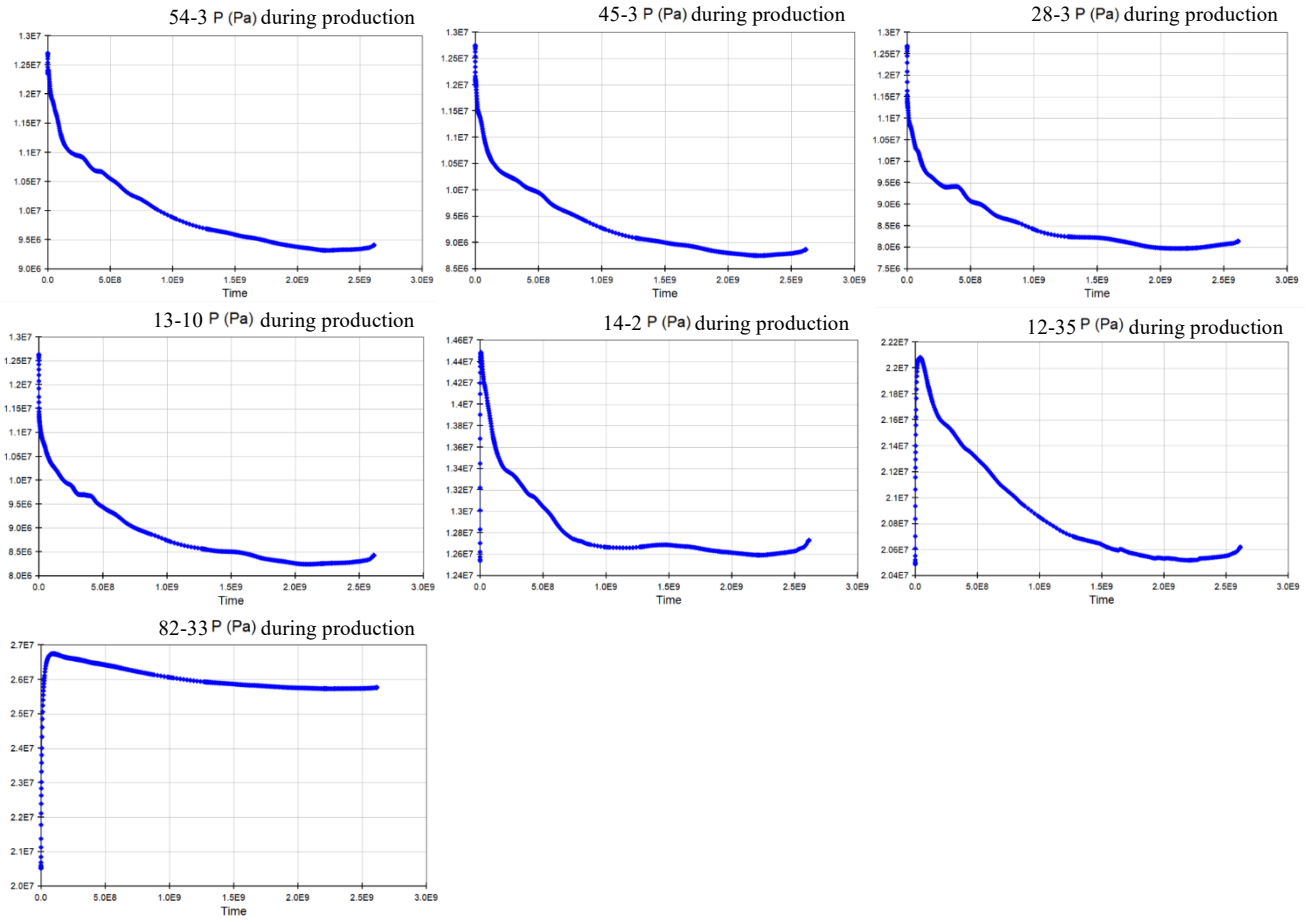

Figure 8: Production model pressure plots versus time in each well. The plot ends when the simulation fails at 83 years (Zebrowski, 2024).

5.3 Sensitivity Analysis and Production Forecasting

To forecast production and assess long-term sustainability at the RHS reservoir, the model was run at the same production rate until simulation failure, which occurred after 83 years. In that time, the steam cap initially continued to expand, particularly in the north-south direction along the OMF, until it stagnated 50 years into the simulation and then started to dissipate, likely due to declining temperatures. Bottom-hole temperatures in each of the geothermal wells also dropped between 0 and 13°C over 83 years (see Figure 7), except for injection well 14-2, which dropped by 95°C over that time. This contrast shows that effective heat mining occurs between well 14-2 and the production wells, which can be observed in Figure 9. Cool 14-2 injectate predominantly sinks prior to recirculating through the reservoir, which is supported by geochemisty data (Simmons, 2021). Although the bottom-hole temperatures did not decline as much as expected, the shallow temperature profiles cooled more significantly. The simulation failed when the depth of the steam cap increased enough that the rate of production could no longer be maintained (Zebrowski, 2024).

A limited sensitivity analysis was also performed on the production model, focusing on permeability. A half-order-of-magnitude increase in permeability was applied to the main reservoir, lower reservoir, and permeable fault regions in both the activation stage of the native state model and the production model. The activation stage was rerun for this sensitivity analysis to ensure stability of the production model initial conditions at the new permeability. After 6,750 years, the higher permeability activation stage well profiles nearly matched the base case conditions, at which point the results were applied to the new production model. The key finding from this sensitivity analysis is that the steam cap extents are shallower in the higher permeability model, while the lateral distribution remains largely the same. The well temperature profiles also show minimal change, with similar bottom-hole temperatures across both models. The steam cap extents for both the base case and high permeability case are shown in Figures 6 (Zebrowski, 2024).

Production forecasting was also tested in the higher permeability case, and the simulation successfully ran for 1,000 years without failure. The shallower steam distribution in the higher permeability case makes it possible for the supplied production rate to be sustained indefinitely (Zebrowski, 2024). However, this assessment does not consider the thermal decline in the reservoir or the sustainability of heat production over time.

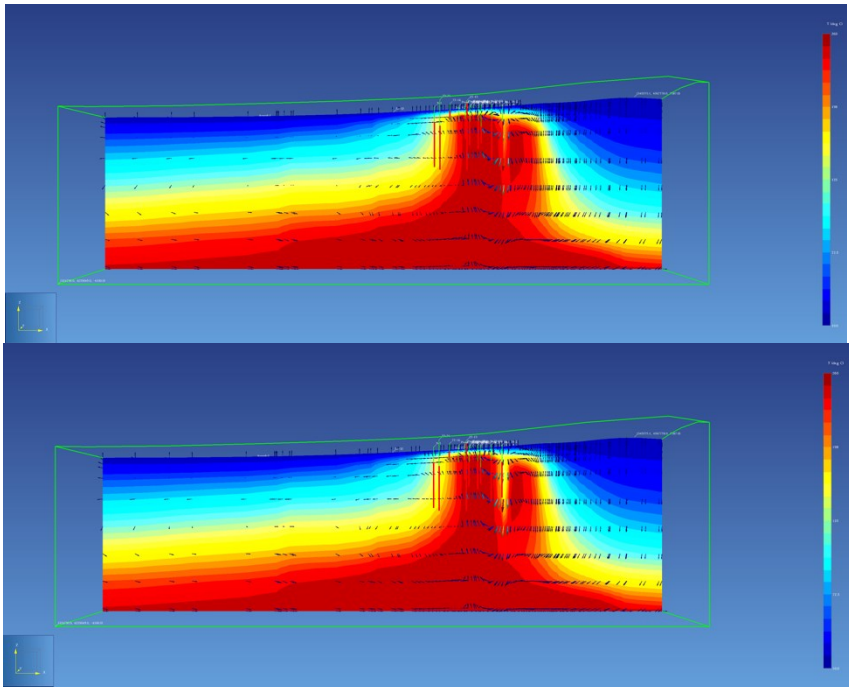

Figure 9: West to east cross-sectional view of the RHS model, sliced at 4,262,300 m northing (near well 14-2) after 41 (top) and 83 (bottom) simulated years. Fluid flow vectors are also shown, which depict a predominantly downward flow of cold reinjection fluid from well 14-2 that then follows a deep recirculation path, improving heat sweep (Zebrowski, 2024).

6. CONCLUSIONS

Native state and production modeling of the Roosevelt Hot Springs hydrothermal system was conducted in TOUGH2. The objectives of the model were as follows:

1. Develop a native state model that reasonably represents the pre-production condition of the reservoir.
2. Use the native state model as the initial conditions for a 40-year geothermal production simulation.
3. Analyze the formation and evolution of the subsurface steam cap as it relates to geothermal production activities and the changing pressure and temperature distributions in the reservoir.

The key conclusions from this modeling effort are two-fold. First, native state modeling of the RHS system necessitates a two-stage approach. An initialization stage, with intermediate reservoir permeability, is required to achieve widely distributed high temperatures at shallow depths. Initialization is followed by an activation stage, where the reservoir permeability increases due to mechanical processes such as fault activation and fractures opening. This activation stage is essential to create suitably high permeability values capable of supporting geothermal production. Both stages are required to create a high temperature, productive reservoir, as is observed at RHS today. The necessity of this two-step process demonstrates that the hydrothermal system is a transient one, and mechanical and chemical effects cannot be neglected when modeling hydrothermal systems over large timescales (Zebrowski, 2024).

Secondly, the production model reveals the formation and expansion of a subsurface steam cap over the permeable faults and western reservoir, which directly correlates with declining reservoir pressures and geothermal production. This finding supports the hypothesis that production activities and pressure decline are the mechanisms behind subsurface steam formation (Zebrowski, 2024).

7. FUTURE WORK

The calibration of the native state and production models can be further refined to better align with observed conditions. The base model presented here was calibrated primarily based on the bottom-hole temperatures in the main reservoir wells, with limited consideration given to wells outside of the reservoir. The temperature match outside of the main reservoir could therefore be further calibrated. In particular, improving the temperature profile match in well 12-35 would be help verify the steam cap behavior in the northern periphery. The model mesh resolution could also be increased (Zebrowski, 2024).

A detailed and systematic sensitivity analysis could be performed on any newly calibrated models. Additionally, different production scenarios and forecasting models could be tested to assess the long-term sustainability of the reservoir, and see how it responds under varying stress conditions. Forecasting of the production model could also be used to evaluate risks associated with reservoir cooling, excessive steam cap expansion, and possible outflow plume reversal. Adding a tracer to the model could enhance the understanding of flow behavior (Zebrowski, 2024).

7. ACKNOWLEDGMENTS

Funding support for this project provided by the U.S. Department of Energy's (DOE) National Energy Technology Laboratory (NETL) through the Carbon Utilization and Storage Partnership (CUSP) under Award No. DE-FE0031837, which is evaluating CO2 storage in EGS systems. I would also like to acknowledge Dave Faulder, Elliot Yearsley, and Han Yu for generously sharing their time, expertise, and data in support of this model.

REFERENCES

Allis, R. G., Gwynn, M., Hardwick, C., Hurlbut, W., Kirby, S. M., & Moore, J. N. (2019). Thermal characteristics of the Roosevelt Hot Springs system, with focus on the FORGE EGS site, Milford, Utah. In R. Allis & J. N. Moore (Eds.), Geothermal characteristics of the Roosevelt Hot Springs system and adjacent FORGE EGS site, Milford, Utah (Utah Geological Survey Miscellaneous Publication 169-D, 22 p.). https://doi.org/10.34191/MP-169-D

Allis, R. G., Gwynn, M., Hardwick, C., Kirby, S. M., Moore, J. N., & Chapman, D. (2015). Re-evaluation of the pre-development thermal regime of Roosevelt Hot Springs geothermal system, Utah. Stanford Geothermal Reservoir Engineering Workshop. Retrieved from https://www.geothermallibrary.org/index.php?mode=pubs&action=view&record=8019519

Allis, R. G., & Larsen, G. (2012). Roosevelt Hot Springs Geothermal field, Utah—reservoir response after more than 25 years of power production. Proceedings, 37th Workshop on Geothermal Reservoir Engineering, Stanford University, 8. Retrieved from https://pangea.stanford.edu/ERE/pdf/IGAstandard/SGW/2012/Allis.pdf

Bamford, R. W., Christensen, O. D., & Capuano, R. M. (1980). Multielement geochemistry of solid materials in geothermal systems and its applications. Part 1. Hot-water system at the Roosevelt Hot Springs KGRA, Utah. https://doi.org/10.2172/5197458

Becker, D. J., & Blackwell, D. (1993). Gravity and hydrothermal modeling of the Roosevelt Hot Springs Area, southwestern Utah. Journal of Geophysical Research: Solid Earth, 98(B10), 17787–17800. https://doi.org/10.1029/93JB01231

Caine, J. S., Evans, J. P., & Forster, C. B. (1996). Fault zone architecture and permeability structure. Geology, 24 (11), 1025. https://doi.org/10.1130/0091-7613(1996)024<1025:FZAAPS>2.3.CO;2

Faulder, D. D. (1991). Conceptual geologic model and native state model of the Roosevelt Hot Springs hydrothermal system. Proceedings, 16th Workshop on Geothermal Reservoir Engineering, p. 131-142. Retrieved from https://pangea.stanford.edu/ERE/pdf/IGAstandard/SGW/1991/Faulder.pdf

Faulder, D. D. (1994). Long term flow test No. 1, Roosevelt Hot Springs. Trans. GRC, 18, p. 583-590. Retrieved from https://www.geothermallibrary.org/index.php?mode=pubs&action=view&record=1007044

Finnila, A., Doe, T., Podgorney, R., Damjanac, B., Xing, P., & Associates, G. (2021). Revisions to the discrete fracture network model at Utah FORGE site. Trans. GRC, 45, p. 757-766.

Forrest, R. J. (1994). Geothermal development at Roosevelt Hot Springs Geothermal Area Beaver County, Utah 1972—1993, 37–44.

Glenn, W. E., & Hulen, J. B. (1979). Interpretation of well log data from four drill holes at Roosevelt Hot Springs KGRA. Univ. Utah Research Inst., Earth Science Lab. Rept. 28, 74 p. Retrieved from https://www.osti.gov/scitech/biblio/5597946

Gwynn, M., Allis, R. G., Hardwick, C., Jones, C., Nielsen, P., & Hurlbut, W. (2019). Compilation of rock properties from FORGE well 58-32, Milford, Utah. In R. Allis & J. N. Moore (Eds.), Geothermal characteristics of the Roosevelt Hot Springs system and adjacent FORGE EGS site, Milford, Utah (Utah Geological Survey Miscellaneous Publication 169-L, 36 p.). https://doi.org/10.34191/MP-169-L

Ingebritsen, S. E., Sanford, W. E., & Neuzil, C. E. (2006). Groundwater in geologic processes (2nd ed.). Cambridge University Press.

Kirby, S. M., Simmons, S., Inkenbrandt, P. C., & Smith, S. (2019). Groundwater hydrogeology and geochemistry of the Utah FORGE site and vicinity. In R. Allis & J. N. Moore (Eds.), Geothermal Characteristics of the Roosevelt Hot Springs System and Adjacent FORGE EGS Site, Milford, Utah. Utah Geological Survey. https://doi.org/10.34191/MP-169-E

Knudsen, T., Kleber, E., Hiscock, A., & Kirby, S. M. (2019). Quaternary geology of the Utah FORGE site and vicinity, Millard and Beaver Counties, Utah. In R. Allis & J. N. Moore (Eds.), Geothermal characteristics of the Roosevelt Hot Springs system and adjacent FORGE EGS site, Milford, Utah (Utah Geological Survey Miscellaneous Publication 169-B, 21 p., 2 appendices). https://doi.org/10.34191/MP-169-B

Lippmann, M. J., & Bodvarsson, G. S. (1985). The Heber geothermal field, California: Natural state and exploitation modeling studies. Journal of Geophysical Research, 90, 745-758.

Lynne, B. Y., Campbell, K. A., Moore, J. N., & Browne, P. R. L. (2005). Diagenesis of 1900-year-old siliceous sinter (opal-A to quartz) at Opal Mound, Roosevelt Hot Springs, Utah, USA: Sedimentary Geology, 179 (3) p. 249–278.

Mason, J. L. (1998). Groundwater hydrology and simulated effects of development in the Milford area, an arid basin in south¬western Utah: U.S. Geological Survey Professional Paper 1409-G.

McKenna, J. R., & Blackwell, D. D. (2004). Numerical modeling of transient Basin and Range extensional geothermal systems. Geothermics, 33, 457–476.

Mesimeri, M., Pankow, K. L., Baker, B., & Hale, J. M. (2021). Episodic earthquake swarms in the Mineral Mountains, Utah driven by the Roosevelt hydrothermal system: Journal of Geophysical Research: Solid Earth, 126, 15 p. e2021JB021659. https://doi.org/10.1029/ 2021JB021659.

Moore, J. N., Allis, R.G., Simmons, S., Nash, G., McLennan, J. D., Forbes, B., Jones, C., Pankow, K., Hardwick, C., Gwynn, M., et al. (2018). Utah FORGE: Final phase 2B topical report; Technical Report, DOE Geothermal Data Repository; Energy and Geoscience Institute at the University of Utah: Salt Lake City, UT, USA.

Moore, J. N., McLennan, J. D., Pankow, K., Simmons, S., Podgorney, R., Wannamaker, P. E., Rickard, W., & Xing, P. (2020). The Utah Frontier Observatory for Research in Geothermal Energy (FORGE): A laboratory for characterizing, creating and sustaining enhanced geothermal systems. Proceedings, 45th Workshop on Geothermal Reservoir Engineering Stanford University. Retrieved from https://gdr.openei.org/files/1146/Moore_UtahFORGE_overview_Stanford_2020.pdf

Moore, J. N., & Nielson, D. L. (1994). An overview of the geology and geochemistry of the Roosevelt Hot Springs geothermal system, Utah, 25–36.

Moore, J. N., Simmons, S., McLennan, J. D., Jones, C., Skowron, G., Wannamaker, P. E., Nash, G., Hardwick, C., Hurlbut, W., Allis, R.G., Kirby, S. M., Erickson, B., Feigl, K., Batzli, Sam, Miller, John, Witter, Jeff, Podgorney, Rob, Pankow, Kristine, Reinisch, E., Patel, V., Martin, T., Rutledge, J., & McKean, A. (2019). Utah FORGE: Phase 2C topical report. United States. https://dx.doi.org/10.15121/1578287

Nielson, D. L., Evans, S. H., & Sibbett, B. S. (1986). Magmatic, structural, and hydrothermal evolution of the Mineral Mountains intrusive complex, Utah. Geological Society of America Bulletin, 97(6), 765. https://doi.org/10.1130/0016-7606(1986)97<765>2.0.CO;2

Podgorney, R. (2020). Utah FORGE: Earth model mesh data for selected surfaces. Geothermal Data Repository. https://doi.org/10.15121/1495398

Podgorney, R., Finnila, A., Simmons, S., & McLennan, J. D. (2021). A reference thermal-hydrologic-mechanical native state model of the Utah FORGE enhanced geothermal site. Energies, 14(16), Article 16. https://doi.org/10.3390/en14164758

Pruess, K., Oldenburg, C., & Moridis, G. (2012). TOUGH2 User's guide, Version 2 (LBNL-43134). Lawrence Berkeley National Laboratory. https://www.lbl.gov/

Sibson, R. H. (2014). Earthquake rupturing in fluid-overpressured crust: How common? Pure and Applied Geophysics, 171, 2867–2885.

Simmons, S. F., Allis, R. G., Kirby, S. M., Moore, J. N., & Fischer, T. P. (2021). Interpretation of hydrothermal conditions, production-injection induced effects, and evidence for enhanced geothermal system-type heat exchange in response to >30 years of production at Roosevelt Hot Springs, Utah, USA. Geosphere, 17(6), 1997–2026. https://doi.org/10.1130/GES02348.1

Sorey, M. L. & Colvard, E. M. (1994). Measurements of heat and mass flow from thermal areas in Lassen Volvanic National Park, California, 1984-93. US Geological Surcey Water Resources Investigations Report, 94-4180-A.

Topex. (n.d.). Data retrieval page. University of California, San Diego. Retrieved April 2024, from https://topex.ucsd.edu/cgi-bin/get_data.cgi

Trow, A. J., Pankow, K. L., Wang, Y., & Lin, F.-C. (2019). Localized ambient noise tomography over the FORGE Utah site. In R. Allis & J. N. Moore (Eds.), Geothermal characteristics of the Roosevelt Hot Springs system and adjacent FORGE EGS site, Milford, Utah (Utah Geological Survey Miscellaneous Publication 169-J, 15 p.). https://doi.org/10.34191/MP-169-J

Wannamaker, P. E., Maris, V., Mendoza, K., & Moore, J. N. (2021). Deep heat and fluid sources for Roosevelt Hot Springs hydrothermal system and potential heat for the Utah FORGE EGS from 3D FORGE and SubTER magnetotelluric coverage. Geothermal Resources Council Transactions, 45. Retrieved from https://www.geothermal-library.org/index.php?mode=pubs&action=view&record=1034421

Wilson, W. R., & Chapman, D. S. (1980). Thermal studies in a geothermal area: Report I. Thermal studies at Roosevelt Hot Springs, Utah. Retrieved from https://www.osti.gov/servlets/purl/7015581

Wilson, W. R., & Chapman, D. S. (1980). Thermal studies in a geothermal area: Report I. Thermal studies at Roosevelt Hot Springs, Utah. Retrieved from https://www.osti.gov/servlets/purl/7015581

Yearsley, E. (1994). Roosevelt Hot Springs reservoir model applied to forecasting remaining field potential. Geothermal Resources Council Transactions, 18. Retrieved from https://www.geothermal-library.org/index.php?mode=pubs&action=view&record=1007049

Yu, H., Xu, T., Yuan, Y., & Feng, G. (2021). Improved preproduction conceptual-numerical model of RHS. Acta Geologica Sinica (English Edition), 95(6), 1805–1815

Zebrowski, A., & McPherson, B. J. (2024). Characterization of thermal ground at the Roosevelt Hot Springs hydrothermal system, Utah. Proceedings, 49th Workshop on Geothermal Reservoir Engineering Stanford University. Retrieved from https://pangea.stanford.edu/ERE/db/Ge°Conf/papers/SGW/2024/Zebrowski.pdf

Zebrowski, A.M. (2024). Characterization of the Steaming Ground at Roosevelt Hot Springs Geothermal System and Evolution of the Subsurface Steam Cap [Master's Thesis, University of Utah]. ProQuest Dissertations and Theses Global.